Molecular Mechanisms of Light Harvesting in the Minor Antenna CP29 in Near-Native Membrane Lipidic Environment

Samim Sardar,[1, #] Roberto Caferri,[2, #] Franco V. A. Camargo,[3] Javier Pamos Serrano,[4] Alberto Ghezzi,[4] Stefano Capaldi,[2] Luca Dall'Osto,[2] Roberto Bassi,[2] Cosimo D'Andrea,[1, 4, *] and Giulio Cerullo,[3, 4, *]

[1]Center for Nano Science and Technology @PoliMi, Istituto Italiano di Tecnologia, 20133 Milan, Italy

[2]Dipartimento di Biotecnologie, Università di Verona, Strada Le Grazie 15, 37134 Verona, Italy

[3]Istituto di Fotonica e Nanotecnologie, Consiglio Nazionale delle Ricerche, Piazza L. da Vinci 32, 20133 Milano, Italy

[4]Dipartimento di Fisica, Politecnico di Milano, Piazza L. da Vinci 32, 20133 Milano, Italy

Corresponding Authors*: cosimo.dandrea@polimi.it, giulio.cerullo@polimi.it

[#]These authors contributed equally.

ABSTRACT

CP29, a chlorophyll (Chl) *a*/*b*-xanthophyll binding protein, bridges energy transfer between the major LHCII antenna complexes and Photosystem II reaction centres. It hosts one of the two identified quenching sites making it crucial for regulated photoprotection mechanisms. Until now, the photophysics of CP29 has been studied on the purified protein in detergent solutions, since spectrally overlapping signals affect *in vivo* measurements. However, the protein in detergent assumes non-native conformations compared to its physiological state in the thylakoid membrane. Here, we report a detailed photophysical study on CP29 inserted in discoidal lipid bilayers, known as nanodiscs, which mimic the native membrane environment. Using picosecond time-resolved fluorescence and femtosecond transient absorption (TA), we observed shortening of the Chl fluorescence lifetime with a decrease of the carotenoid triplet formation yield for CP29 in nanodiscs as compared to the protein in detergent. Global analysis of TA data suggests a ^{1}Chl* quenching mechanism dependent on excitation energy transfer (EET) to a carotenoid dark state, likely the proposed S*, which is believed to be formed due to a carotenoid conformational change affecting the S_1 state. We suggest that the accessibility of the S* state in different local environments plays a key role in determining the quenching of Chl excited states. *In vivo*, non-photochemical quenching is activated by de-epoxidation of violaxanthin into zeaxanthin. CP29-Zeaxanthin in nanodiscs further shortens Chl lifetime, which underlines the critical role of zeaxanthin in modulating photoprotection activity.

KEYWORDS: Photosynthesis, CP29, nanodiscs, Non-Photochemical Quenching, energy transfer.

I. INTRODUCTION

In oxygenic photosynthesis, the conversion of sunlight into chemical energy occurs upon light absorption by pigment-protein complexes known as the light-harvesting complexes (LHCs), embedded in the thylakoid membrane. LHCs efficiently transfer the excitation energy to the reaction centre where it initiates charge separation and fuels electron transport steps which lead to the reduction of $NADP^+$ and the synthesis of ATP, needed for CO_2 absorption and sugar synthesis by the Calvin-Benson cycle. The mechanisms of these excitation energy transfer (EET) processes have been extensively studied, and are now rather well understood.[1–6]

Besides light harvesting, LHCs play a key role in protecting photosynthetic organisms from dangerous processes triggered by excessive absorption. High irradiance, exceeding the maximal capacity for photochemical reactions, leads to intersystem crossing (ISC) and production of triplets (^{3}Chl*) which, in turn, react with O_2 to yield singlet oxygen ($^1O_2$*) and photoinhibition.[7] Plants and algae have evolved photoprotective mechanisms to prevent photodamage, among which the most impressive is Non-Photochemical Quenching (NPQ)[8,9], which harmlessly dissipates excessive photoexcited states as heat, thus preventing them from triggering unwanted photochemical reactions and charge recombination. NPQ is catalysed within LHC proteins, including CP29, through switching from a light harvesting to a dissipative quenched state, closely following changes in irradiance.

Like all LHCs, CP29 binds chlorophyll (Chl) *a*, Chl *b* and carotenoids (Cars) of the xanthophyll family. The lowest energy Q bands of Chls absorb in the red, with peaks at 678 nm (Q_y band of Chl *a*), 640 nm (Q_y band of Chl *b*), shoulder around ~ 590-620 nm (Q_x band of Chl *a*, the assignment of this band is being debated[10–12]) and 590 nm (Q_x band of Chl *b*). The Chls also display absorption in the 430-470 nm wavelength range, the so-called Soret or B band. Cars only

absorb in the blue-green region of the spectrum, with their lowest energy transitions peaking at 480-510 nm, and display a peculiar photophysics, with the lowest energy singlet excited state (S_1) being optically dark,[13] so that it does not appear in the linear absorption spectrum. The first optically allowed transition is therefore to the second excited state S_2, from which relaxation to the dark S_1 state occurs on the ≈100-fs timescale through an internal conversion (IC) process; the S_1 state, in turn, relaxes non-radiatively to S_0 on the ≈10-ps timescale through a second IC process.

Cars play several roles in photosynthesis by: (i) acting as accessory light-harvesting pigments, which transfer their photoexcitation energy to Chls; (ii) protecting the photosynthetic apparatus via quenching ^{3}Chl* and $^1O_2$*; (iii) being needed for the fastest component of the NPQ process, known as qE, which dissipates ^{1}Chl* in excess. Several molecular mechanisms have been proposed for the qE process, some of which may be mutually non-exclusive and act concertedly: energy/electron transfer between Chls and Cars[14–19], excitonic mixing of Chls and Cars[20–22] or interactions between Chls[23–25]. In recent years, genetic manipulation of qE-related proteins in land plants has shown promise towards enhancing light and water use efficiency.[26,27] However, the detailed molecular mechanism underlying photoprotection is still unclear[28], which is limiting the exploitation of its full potential in improving plant and algal productivity.

The photoinduced processes in LHCs have been studied in detail using a variety of time-resolved optical spectroscopies, such as time-resolved photoluminescence (TRPL),[29–31] femtosecond transient absorption (TA)[13,32,33] and two-dimensional electronic spectroscopy.[34–36] However, since *in vivo* spectroscopy on leaves and thylakoid membranes is hindered by strong scattering and by the presence of many spectrally overlapping signals, the studies are typically performed on isolated LHCs extracted from intact systems and solubilized using detergents. Unfortunately, detergents provide a local environment that is dramatically different with respect

to that of the thylakoid membrane. This may introduce non-native protein conformational changes and subtle changes in pigment–pigment as well as pigment–protein orientations and distances, influencing the photophysics of the complex.[37] An approach to solve this problem is the use of nanodiscs, which are discoidal lipid bilayer membranes, mimicking the near-native membrane environment. Recently, Son et al.[38,39] reported differences of up to 40% in the EET timescales within the LHCII complex embedded in nanodiscs and in detergent, indicating a strong influence of the environment on photophysics.

CP29 is one of the monomeric LHCs of plants and algae; it contains ~13-14 Chls (around 10 Chl *a* and 4 Chl *b*) and 3 Cars, namely violaxanthin (Vio), neoxanthin (Neo) and lutein (Lut). CP29 plays an important role in the EET transfer pathways within Photosystem II (PSII) supercomplexes, because of its pivotal location connecting the CP47 subunit of PSII core complex to the outer LHCII and CP24 antenna subunits, hosting the largest pigment complement. CP29 also plays a crucial role in photoprotection since it catalyses qE, which is triggered by the detection of low luminal pH. Indeed, under excess irradiation the ATPase enzyme activity is inhibited from lack of its ADP substrate, impairing H^+ backflow to the stroma and causing lumen acidification. This activates both enzymes violaxanthin de-epoxidase, leading to zeaxanthin (Zea) synthesis[40], and PSBS, a pigment-less subunit which interacts with CP29 and induces conformational changes leading to quenching[41]. Such CP29 conformational change brings Chls a603, a609 and Zea bound to the L2 site in close contact, activating a dissipative channel.[42] Chl a616, in addition, is involved in the propagation of the quenching to the PSII core.[43,44] Due to the interactions between the Zea S_1 dark state and Chl Q_y excited states, it has been suggested that Zea is directly involved in Chl quenching via the qE mechanism.[20,45]

Here, we combine picosecond TRPL and femtosecond TA spectroscopy to investigate the ultrafast photophysics of CP29 from *Arabidopsis (A.) thaliana* inside nanodiscs and compare the results to those obtained in detergent environment. Following Chl photoexcitation, we observed faster Chl fluorescence decay and a corresponding reduction in the Car triplet formation yield for CP29 in the nanodiscs as compared to the detergent. To understand the role of Zea in the NPQ process, we compared the photophysics of nanodisc-embedded CP29 with Vio *vs.* Zea. Our observations shed light on the influence of local environment on the photophysics of CP29, elucidating the importance of reproducing a near-native environment when studying the molecular mechanisms underlying the photoinduced dynamics.

II. MATERIALS AND METHODS

A. Sample Preparation

The detailed sample preparation procedures, including MSP 1E3D1 overexpression, purification and tag cleavage by TEV protease, CP29-Vio and CP29-Zea over-expression in *A. thaliana* and purification, the assembly of CP29 within nanodiscs, are described in the Supporting Information (SI).

B. Spectroscopic characterization

Linear absorption and fluorescence spectra. Absorption spectra were collected at room temperature (RT) using a SLM Aminco DW-2000 spectrophotometer in buffer containing Hepes 50 mM, NaCl 0.15 M, glycerol 20%, pH 7.5 (and 0.03% α-DM in detergent samples). Fluorescence spectra were acquired using a Jobin–Yvon Fluoromax-3 spectrofluorometer. RT spectra were obtained in buffer containing Hepes 50 mM, NaCl 0.15 M, pH 7.5 (and 0.03% α-DM in detergent samples) (0.02 max OD in Q_y region).

Time-resolved photoluminescence. TRPL measurements[46] were performed using a 40 MHz mode-locked super-continuum fiber laser (Fianium Inc., SC-450) emitting pulses of about 30 ps full width at half maximum (FWHM). A band-pass filter (10 nm FWHM) centered at 630 nm (Thorlabs, Inc.) was employed to spectrally filter the laser beam, which is coupled to a graded-index fiber (100 µm diameter) followed by a lens to focus the beam onto the sample. The sample was concentrated at OD/cm 0.1 on an optical path-length of 0.3 cm. A 650 nm long-pass filter was used before the detection to remove the excitation pulses. The detection system consists of a spectrometer (Acton, sp-2151i, Princeton Instruments) coupled to a 16-channel photo-multiplier tube (PML16-C, Becker & Hickl) connected to a time-correlated single-photon counting (TCSPC, SPC130EM, Becker & Hickl) board. The overall instrumental response function (IRF) of the detection chain has a FWHM of about 200 ps. During all TRPL measurements, the samples were kept at 10°C.

Transient absorption. TA measurements[30,47] were performed using a home-built setup based on a regeneratively amplified Ti:Sapphire laser (Libra, Coherent) emitting 100-fs pulses at 800 nm wavelength and 1 kHz repetition rate. An optical parametric amplifier was employed to generate ~80-fs pulses with ≈10-nm bandwidth at central wavelengths of 630 nm and 510 nm, resonant with the Chls and the Cars, respectively. White-light continuum generation was used to obtain a broadband probe beam (470-700 nm) by focusing the fundamental wavelength pulses in a 2-mm-thick sapphire plate. Appropriate filters were used to reject the remaining light at 800 nm. The transmitted probe after the sample was sent to a spectrometer (SP2150 Acton, Princeton Instruments) and detected using a linear image sensor driven and read out by a custom-built board (Stresing Entwicklungsburo).[48] For each probe wavelength, the differential transmission ($\Delta T/T$) was measured as a function of the pump-probe delay. The pump and probe pulses were spatially

overlapped on the sample at magic-angle (54.7°) polarization. The spatial profiles of pump and probe beams were imaged at the overlap position using a camera before each measurement, and the obtained cross-sections were used to calculate the fluence. The pump fluence was adjusted to 3-5 μJ/cm^2 (0.95×10^{13} – 1.59×10^{13} photons/cm^2), a regime in which bimolecular exciton-exciton annihilation processes are negligible. During all TA measurements, the samples were kept at 10°C. In order to avoid any possible sample degradation during measurements, the signal levels of different TA scans were compared and no degradation was observed for the reported TA data.

Global analysis. Spectro-temporal data matrices acquired from the TA measurements were fitted globally using the Glotaran software program.[49] A sum of exponential functions were used to fit the TA data with a numerical deconvolution of the IRF and a polynomial to describe the chirp of the probe. The fitting of the experimental data was optimized until no systematic residuals were present both in the time and wavelength variables.

III. RESULTS AND DISCUSSION

Figure 1a shows the three-dimensional structure of CP29. Figure 1b presents a schematic illustration of CP29 within a membrane nanodisc or solubilized in detergent. The absorption spectra of CP29-Vio in detergent and in nanodiscs (normalized to the area in the 560 to 720 nm range) have similar profiles, as shown in Figure 1c. However, the difference absorption spectra, shown in the lower panel of Figure 1c, highlight minor changes in both Chls and Car bands, indicating a change in pigment arrangement influenced by the nanodiscs. The absorption spectrum of CP29-Zea exhibits a redshift in the Car S_2 (0–0) absorption (around 490-500 nm) compared to CP29-Vio, as the conjugation length increases upon de-epoxidation.[50] The differences observed in

the Q_y region can be attributed to the changes in the protein-Chl interaction due to the Zea-dependent conformational changes, as Cars do not absorb in the 600-700 nm range.

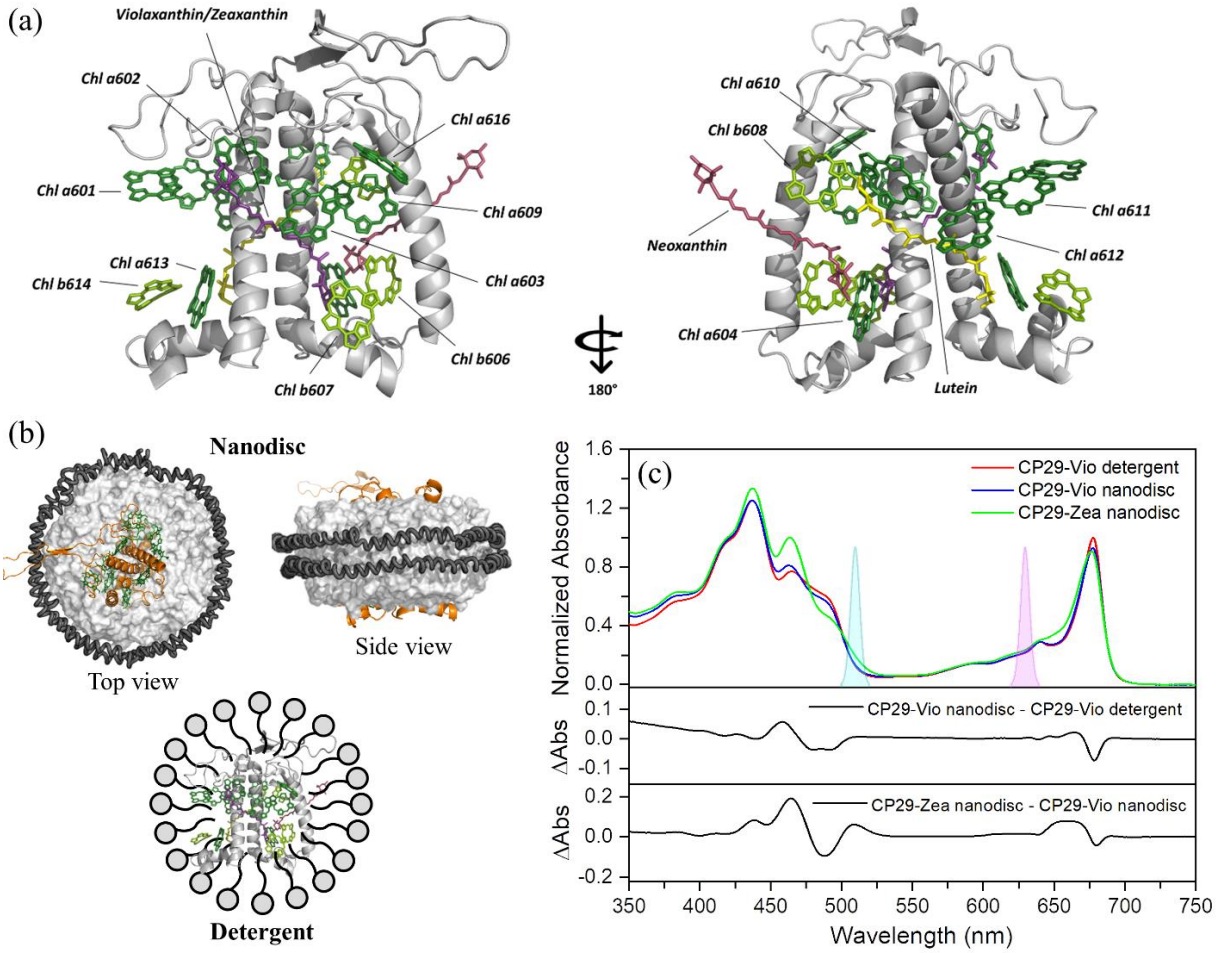

Figure 1: Structure and absorption of CP29. (a) Three-dimensional structure of CP29 from *pisum sativum* (PDB file: 5XNL[51]). Two sides of the protein are shown to display all the bound pigments. For simplicity, Chls are represented by porphyrin groups only. The polypeptide backbone is depicted in grey; Chl *a* in dark green; Chl *b* in light green; Vio in purple; Lut in yellow; and Neo in pink. (b) Schematic illustration of CP29 inside membrane nanodisc (top) and solubilized in detergent (bottom). (c) Normalized steady-state absorption spectra of CP29-Vio in detergent, CP29-Vio in nanodisc and CP29-Zea in nanodisc. Difference absorption spectra are shown at the bottom. The cyan and magenta spectra represent the excitation at 510 nm and 630 nm to selectively pump Car and Chl, respectively.

Figure 2a reports normalized TRPL traces of CP29-Vio in detergent, CP29-Vio in nanodiscs and CP29-Zea in nanodiscs upon excitation at 630 nm, integrated over the 650−750 nm wavelength range. All the TRPL decays are fitted well with three lifetime components and the

timescales are shown in Table 1. The observed lifetimes of CP29 can be attributed to the presence of different emissive states, in agreement with the literature.[29,33] In the case of CP29-Vio in detergent, the long component (4.2 ns) gives the largest contribution to the lifetime (89%), whereas small fractions are found in slightly (1.8 ns, 6%) and strongly (0.37 ns, 5%) quenched states. The time-gated fluorescence spectra shown in Figure S1 in the SI are similar, indicating that the terminal emitter domain of all samples is identical.[52] From this observation, it can be concluded that the quencher in CP29-Vio in detergent could be a non-emissive (dark) state populated from Chl excited states.[33] The fluorescence lifetime of CP29-Vio in nanodiscs is significantly quenched (~20%) compared to the CP29-Vio in detergent (Table 1). The contribution of moderately quenched states (1.8 ns) increases from 6% to 25%, confirming the strong influence of the environment on the quenching efficiency. The Chl fluorescence is further quenched in the presence of Zea, where the contributions of moderately quenched states (2 ns) is enhanced to 68%. The quenching observed in CP29-Zea in nanodiscs compared to CP29-Vio in nanodiscs can be attributed either to the presence of additional quenching sites or to conformational changes in CP29 induced by Zea, as in both cases CP29 is within a membrane-like environment.

Table 1: Time constants and corresponding amplitudes obtained by tri-exponential fits of the fluorescence decays.

Sample	**τ_1 (A_1)**	**τ_2 (A_2)**	**τ_3 (A_3)**	**τ_{avg}**
CP29-Vio detergent	4.25 ns (89.0%)	1.79 ns (6.0%)	0.37 ns (5.0%)	3.90 ns
CP29-Vio nanodisc	3.95 ns (69.8%)	1.83 ns (25.0%)	0.22 ns (5.2%)	3.23 ns
CP29-Zea nanodisc	3.43 ns (30.0%)	2.05 ns (67.7%)	0.19 ns (2.3%)	2.42 ns

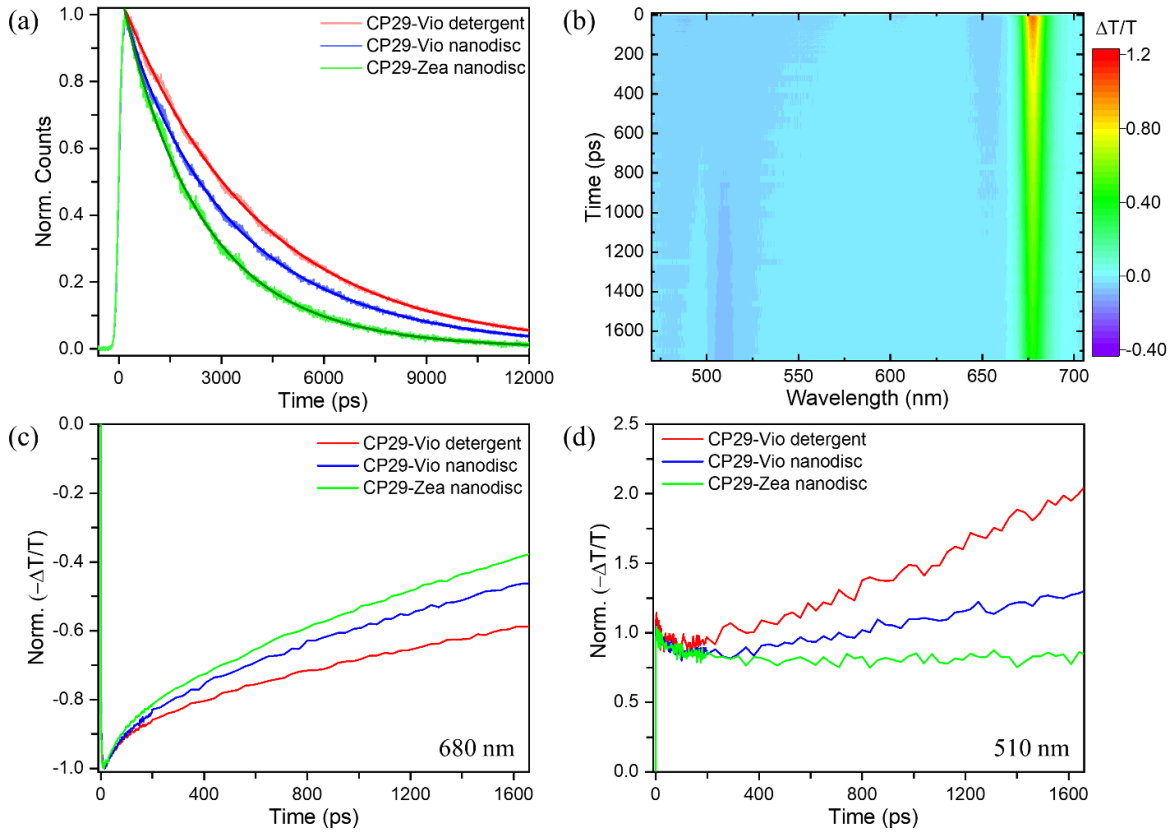

Figure 2: TRPL and TA. (a) Fluorescence lifetime traces of CP29-Vio in detergent, CP29-Vio in nanodiscs and CP29-Zea in nanodiscs at 10ºC. The samples were excited at 630 nm and the emission signal is integrated between 650−750 nm. The dark lines are tri-exponential fits to the data. (b) TA map of CP29-Vio in nanodiscs (pumped at 630 nm). TA kinetics at 680 nm (c) and 510 nm (d) are shown for all three samples.

To investigate the Chl quenching mechanisms, we have employed TA spectroscopy, which is also sensitive to non-emitting states. Figure 2b shows the TA map of CP29-Vio in nanodiscs following selective Chl excitation at 630 nm (see Figure S2 in the SI for TA spectra at selected time delays for all samples). We have performed fluence dependent measurements in order to keep the excitation fluence below the threshold for non-linear effects, such as the formation of transient quenchers and singlet-singlet annihilation.[53] The fluence dependent kinetics at 680 nm upon excitation at 630 nm for all the samples are shown in Figure S3 in the SI. We have selected the pump fluences of 3.6 μJ/cm^2, 5.3 μJ/cm^2 and 4.7 μJ/cm^2 for CP29-Vio detergent, CP29-Vio in nanodiscs and CP29-Zea in nanodiscs, respectively.

The TA map shown in Figure 2b exhibits a strong peak around 680 nm due to ground-state bleaching (GSB) and stimulated emission (SE) of the Chl *a* singlet excited state (^{1}Chl *a**). The TA kinetics at 680 nm for all the three samples are shown in Figure 2c. The traces are in good agreement with the TRPL data, exhibiting faster GSB/SE decay in nanodiscs compared to detergent. On the contrary, the TA kinetics at 640 nm at early timescales (reported in Figure S4 in the SI), which represent the EET from Chl *b* to Chl *a*, show slower decay in nanodiscs compared to detergent. As minor perturbations to inter-pigment distances can have significant impact on the EET dynamics, the slower dynamics observed for Chl *b* to Chl *a* EET suggests that the specific pigments involved might move further apart in nanodiscs as compared to detergent. While the overall structure of the CP29 protein is expected to become more compact in the nanodiscs as compared to the detergent, it may well be that in the new structure the distance of specific pigments increases; alternatively, the lower EET dynamics may be due to a relative rotation of the transition dipole moments of the chromophores. A similar slow-down of the Chl *b* to Chl *a* EET process has also been observed for the LHCII complex in nanodiscs.[38]

In order to investigate the quenching of ^{1}Chl*, we looked at the region of the TA spectrum from 450 to 600 nm. As we selectively pumped Chls at 630 nm rather than directly exciting the Cars, any signal from the Car molecules must be due to an interaction of ^{1}Chl* with Cars. As shown in the inset of Figure S2 in the SI, TA spectra from 450 nm to 600 nm exhibit a broad and rather featureless band due to the excited state absorption (ESA) of ^{1}Chl* and also contain evidence of the Car GSB (peaking at 500 nm) and, for long delays, the Car triplet−triplet ESA (peaking at 510 nm).[45,54] The ESA signal build-up at 510 nm observed on the nanosecond timescale can be attributed to the formation of the Car triplet state (^{3}Car*), by a triplet−triplet EET from the Chl triplet state (^{3}Chl*), which in turn is formed from the ^{1}Chl* by ISC.[55,56] Thus, the buildup of the

^{3}Car* signal is related to the ^{1}Chl* lifetime, i.e. the longer is the ^{1}Chl* lifetime, the larger the fraction of ^{3}Car* states which is formed. Figure 2d shows the TA traces at 510 nm, revealing significantly less formation of ^{3}Car* in nanodiscs compared to the detergent sample. These observations correlate well with the ^{1}Chl* lifetime data shown in Figure 2a.

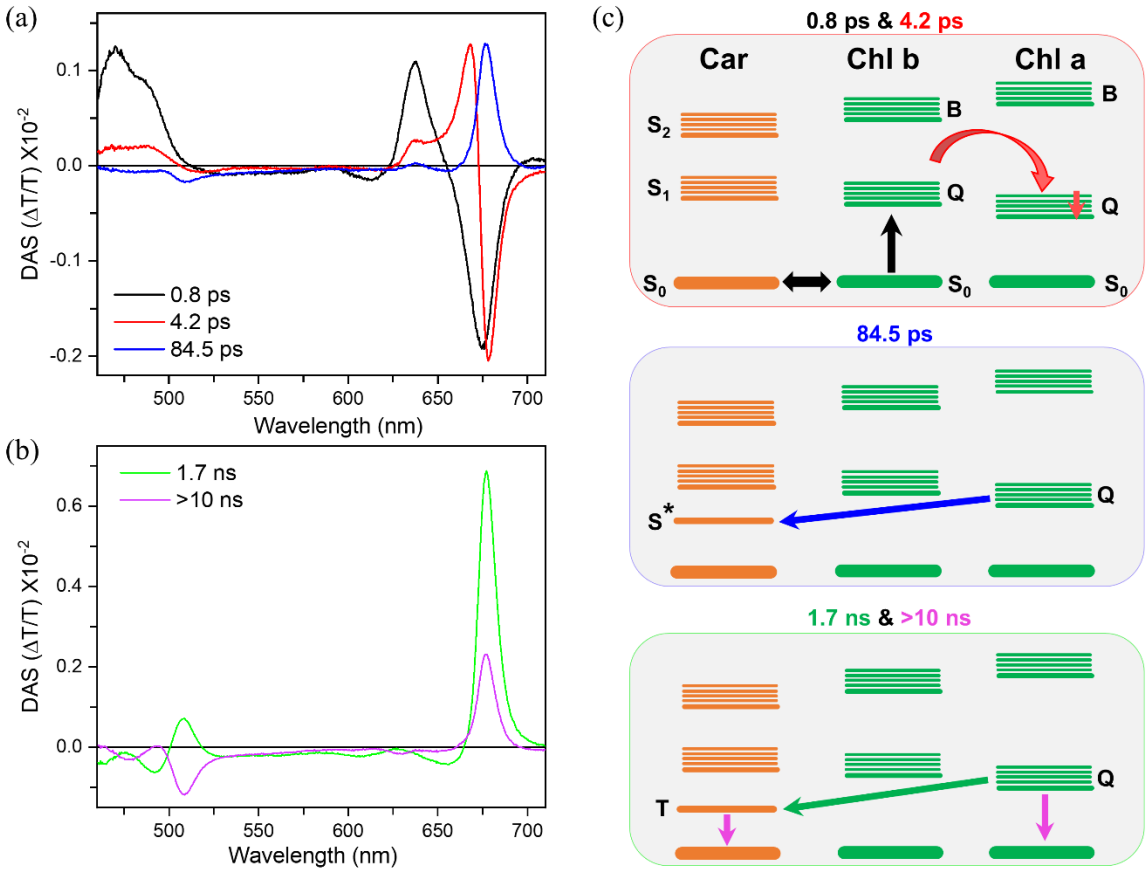

Figure 3: Global analysis of CP29-Vio nanodisc upon excitation at 630 nm. DAS resulting from global analysis of TA data of CP29-Vio in nanodiscs upon excitation at 630 nm reveal five components: (a) first 3 components; (b) last 2 components. (c) Energy level diagrams (not to scale) illustrate the main photophysical processes at different time delays. The double sided arrow in the top panel indicates coupling between Car-Chl b.

To understand in detail the photophysical processes involved in ^{1}Chl* deactivation, we have performed global analysis of the TA data. Figures 3a and 3b show the decay-associated spectra (DAS) for CP29-Vio in nanodiscs. A DAS spectrum consists of the wavelength dependent

amplitude of a given exponential component of the global fit. Hence, it represents how much the TA signal grows or decays on each timescale and for each wavelength, helping correlate bands that evolve together. A negative DAS amplitude means an increasing ΔT/T (rise in GSB/SE or decay in ESA) whereas a positive DAS means a decreasing ΔT/T (decay in GSB/SE or rise in ESA). The TA data of CP29-Vio in nanodiscs following 630 nm excitation was adequately fitted with five components. The first DAS with 800 fs time constant shows signals at 470 nm, 494 nm, 640 nm, and 678 nm. The signals at 470 nm (B band) and 640 nm (Q_y band) correspond to the decay of Chl *b* GSB (positive DAS) whereas the signal at 494 nm represents the Car GSB decrease. We note that, since photoexcitation at 630 nm is out of resonance with Cars, the signals observed at 494 nm at time zero are due to a coupling between Car and Chl *b*, as reported in previous studies.[13,21,57] Hence, the depopulation of the coupled excited state results in a decreased GSB of both Chl *b* and Car (S_2 band at 494 nm). The negative DAS at 678 nm corresponds to an increase in the GSB of the Q_y band of Chl *a*, which acts as acceptor, as schematically shown in Figure 3c.

The second DAS with 4.2 ps time constant (red line in Figure 3a) has similar features as the previous DAS. However, the decrease of GSB in both Chl *b* and Car at lower rates can be attributed to the involvement of red Chl *b*. Different timescales for Chl *b* → Chl *a* EET depending on the involvement of blue Chl *b* (~100s fs) or red Chl *b* (few ps) have been reported in the literature.[58–62] The 4.2 ps DAS also exhibits a derivative lineshape at 675 nm, corresponding to a red shift of the GSB/SE of Chl *a*, a signature of intramolecular vibrational relaxation (IVR) within Chl *a*.

The third DAS at 84 ps (blue line in Figure 3a) shows a positive band around 678 nm, revealing a GSB decrease in Chl *a*. This component is in agreement with the fastest observed lifetime component from the TRPL measurements, considering that the obtained 200-ps value is close to the IRF of the apparatus. Moreover, the DAS contains a weak negative peak at 510 nm.

At 84 ps, the possibility of a depopulating Car Triplet can be ruled out. However, there is the possibility that the quencher spectrum can have the characteristics of a Car S_1 state. To verify this possibility, we have performed TA upon direct Car excitation to obtain the TA spectrum of S_1, which will be discussed later. In this context, the observed signals do not contain any clear indication of having electrochromic shift of the carotenoid S_2 state, which is reported in the literature for other Chl-Car systems.[63,64]

The next DAS with 1.7 ns time constant (green line in Figure 3b) shows the decrease of Chl *a* GSB (positive peak at 678 nm) and the build-up of the Car triplet state ESA at 510 nm. In addition, a clear increase in Car GSB (negative peak at 494 nm) confirms the energy transfer according to the scheme ^{1}Chl*→ ^{3}Chl*→ ^{3}Car*.

The last DAS component represents the decay of excited Chl *a* Q_y and Car T_1 to their respective ground states over timescales much longer than the experimental time window. One should notice that, due to the limited time window over which the TA data are acquired, an accurate determination of the time constants of the long-lived DAS is not possible. We also performed global analysis of the TA data of the other two samples and the DAS for CP29-Vio in detergent and CP29-Zea in nanodiscs are shown in Figure S5. Both samples exhibit similar photophysical processes as CP29-Vio in nanodiscs, although the timescales differ slightly, as shown in the Table 2.

Table 2: Time constants from the Global Analysis of the TA data upon excitation at 630 nm.

Sample	τ_1 (ps)	τ_2 (ps)	τ_3 (ps)	τ_4 (ps)	τ_5
CP29-Vio detergent	0.66	4.3	65.0	1880	>10 ns
CP29-Vio nanodisc	0.80	4.2	84.5	1700	>10 ns
CP29-Zea nanodisc	0.69	4.1	64.0	1750	>10 ns

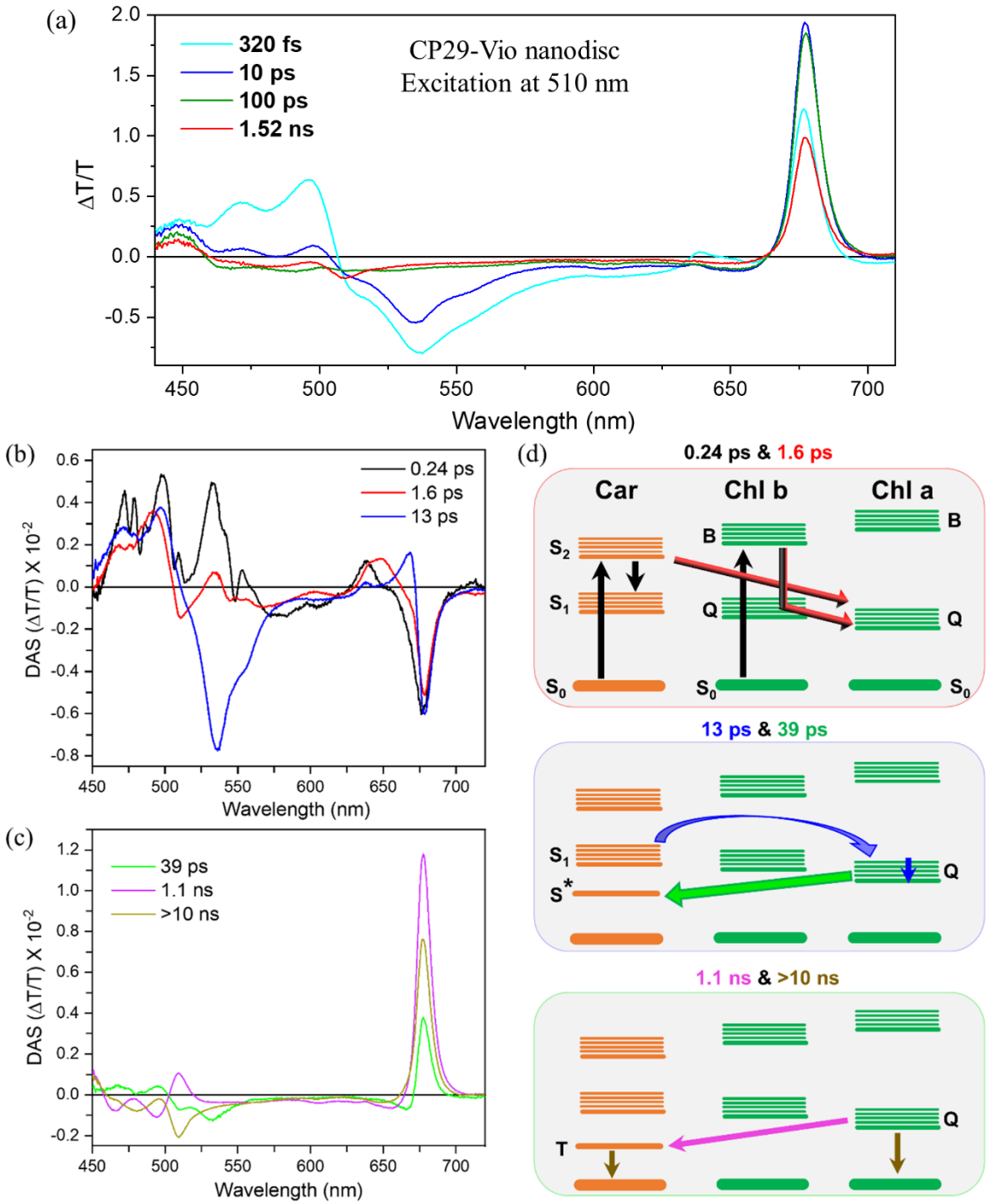

Figure 4: TA and Global analysis of CP29-Vio nanodisc upon excitation at 510 nm. (a) TA spectra at selected time delays for CP29-Vio in nanodiscs. The pump fluence was 27.1 μJ/cm^2. The DAS reveal six components: (b) first 3 components; (c) last 3 components. (d) Energy level diagrams (not to scale) illustrate the main photophysical processes at different time delays.

We have also performed the TA measurements upon excitation at 510 nm, which is mainly resonant with the Car S_2 state. In this case the photoexcitation scenario is much richer and involves the following processes: (i) IC from the Car bright S_2 state to the dark S_1 state; (ii) EET from the S_2 state of Cars to Chls; (iii) IVR within the hot Car S_1 state; (iv) IC from the Car S_1 state to the ground state S_0; (v) EET from the S_1 state of Cars to Chls; (vi) radiative decay of the Chls and formation of ^{3}Car* via ISC. TA spectra at selected time delays for CP29-Vio in nanodiscs upon excitation at 510 nm are shown in Figure 4a. The TA spectra for CP29-Vio in detergent and CP29-Zea in nanodiscs are shown in Figure S6. The DAS for CP29-Vio in nanodiscs, shown in Figure 4b and 4c, reveal six main components.

The first DAS at 241 fs shows the decay of the GSB of Chl *b* (640 nm) and GSB of Car (495 nm) and the build-up of Car S_1 ESA band at 535 nm and Chl *a* GSB at 678 nm. This DAS contains the $S_2 \rightarrow S_1$ IC process in the Cars, EET from Cars S_2 state to Chl *a* and from Chl *b* to Chl *a*. The photophysical processes are schematically displayed in Figure 4d.

The second DAS at 1.6 ps exhibits similar features as the previous one and can be assigned to EET from the hot S_1 state of Cars to Chl *a*, resulting in a decay of Cars GSB and a build-up of Chl *a* GSB.

The next DAS at 13 ps shows a decrease of Car GSB at 495 nm and S_1 ESA at 535 nm and an increase in Chl *a* GSB at 678 nm and corresponds to the IC of the vibrationally relaxed Car S_1 to S_0 in parallel with EET from S_1 to the Chl *a* Q_y bands. It also contains some IVR in the Q_y state of Chl *a*, with its characteristic derivative lineshape.

The DAS at 39 ps, besides some residual Car decay, exhibits a quenching of the Chl *a* Q_y band similar to the fast component observed upon excitation at 630 nm, including the negative peak at 510 nm. It is to be noted that the peak at 510 nm is observed at a shorter wavelength and

clearly separated from the characteristic ESA of the Car S_1 state as evident from the plot shown in Figure S8 for the DAS obtained upon different excitation wavelength. Although the quencher spectrum resembles that of the Car triplet, it possesses a lifetime (few tens of picoseconds) similar to that of a Car singlet excited state.[50] The quencher species can be attributed to the Car S* state which has previously been reported in the literature for many other Cars in solution[65–68] and in LHCs[69–71]. Recently, it has been demonstrated in a LHC binding astaxanthin that the Chl excitation is quenched by the astaxanthin S* state, which becomes accessible via a twist of the carotenoid end-ring.[72] Mascoli et al.[33] have observed a similar quencher in detergent-solubilized monomeric CP29, and by applying a heterogeneous model to TA measurements, they assigned it to a carotenoid S* state. Although the existence of Car S* state is very well documented in the literature, the origin of this state is still debated. It has been interpreted both as hot ground state signal[73] and as a separate electronic state[74] as well. Balevičius Jr et al.[75] have illustrated the dual origin of the S* signal as absorption from the hot ground state such as both non-equilibrium vibronic populations and increased local temperature before IVR is over and the S* signal indicates increased local temperature only at times exceeding IVR.

The last two DAS at 1.1 ns and >10 ns show the build-up of Car triplet and the decay of excited Chl *a* Q_y and Car T_1 to their respective ground states, respectively. DAS for CP29-Vio in detergent and CP29-Zea in nanodiscs upon 510 nm excitation also exhibit similar processes, as shown in Figure S7. We can speculate that the enhanced quenching of Chl excited states within nanodiscs compared to the detergent can be related to the greater accessibility of the S* state in the near native environment. Consistently, it can be suggested that the enhanced quenching in CP29-Zea vs CP29-Vio, both in nanodiscs, might well derive from an increased accessibility of the carotenoid (Zea) S* state to ET from Chl a.

IV. CONCLUSION

In this work, we have analyzed the photophysical processes in CP29 inside nanodiscs using the combination of TRPL and TA. CP29 in a near-native membrane environment is in a significantly quenched state compared to when it is solubilized in detergent. This observation confirms that the local environment plays a key role in determining the conformation and dynamics of the photosynthetic complexes. Global analysis of the TA data reveals the photoinduced processes at different time delays. It suggests a possible excitation energy transfer from the Chl *a* Q_y to a Car dark state S*, which is generated due to conformational changes in the Car S_1 state. The formation of the S* state is further confirmed by performing TA measurements upon selectively exciting the Car at 510 nm. We have also investigated the role of Zea in the photoprotection mechanism of CP29 in nanodiscs, which exhibit enhanced quenching of Chl emission in the presence of Zea. Light harvesting proteins undergo several quenching mechanisms[76] including qE, which is activated by low luminal pH and qZ, which depends on the synthesis of Zeaxanthin. The system we have analysed here, includes Zea but not the pH sensor PSBS, and is therefore relevant for the understanding of the pH-independent, Zea dependent type of quenching.[77] The nanodisc system, however, is open to the possibility of including, besides CP29, also PSBS, allowing for analysis of the qE component of the quenching. Finally, the verification of the role of individual chromophores in the processes discussed above, will rely on ultrafast spectroscopy studies on CP29 mutants[42], affected on pigment binding sites, to be performed.

SUPPORTING INFORMATION

See the supplementary material for sample preparation and Figures S1–7.

ACKNOWLEDGEMENTS

G.C. and L.D. acknowledge the support from the PRIN 2017 Project 201795SBA3−HARVEST. We would like to thank Prof. Gabriela Schlau-Cohen for advice in the procedures for preparation of nanodiscs.

AUTHOR CONTRIBUTIONS

R.B., C.D.A. and G.C. conceived the project and supervised the experimental activities. R.C. and S.C. prepared the samples under the supervision of L.D.O.. S.S. and A.G. performed the TRPL experiments. S.S. and F.V.A.C. performed the TA experiments. J.P.S. and F.V.A.C. performed the global analysis. All authors contributed to the data interpretation and to the writing of the manuscript.

COMPETING INTERESTS

The authors declare that the research was conducted in the absence of any commercial or financial relationships that could be construed as a potential conflict of interest.

REFERENCES

[1] T. Mirkovic, E.E. Ostroumov, J.M. Anna, R. Van Grondelle, Govindjee, and G.D. Scholes, Chem. Rev. **117**, 249 (2017).

[2] R. Croce and H. van Amerongen, Nat. Chem. Biol. **10**, 492 (2014).

[3] R. van Grondelle and V. I. Novoderezhkin, Phys. Chem. Chem. Phys. **8**, 793 (2006).

[4] V.I. Novoderezhkin and R. van Grondelle, Phys. Chem. Chem. Phys. **12**, 7352 (2010).

[5] T. Renger, Photosynth. Res. **102**, 471 (2009).

[6] G.D. Scholes, G.R. Fleming, A. Olaya-Castro, and R. Van Grondelle, Nat. Chem. **3**, 763 (2011).

[7] J. Barber and B. Andersson, Trends Biochem. Sci. **17**, 61 (1992).

[8] K.K. Niyogi, Curr. Opin. Plant Biol. **3**, 455 (2000).

[9] A. Pinnola and R. Bassi, Biochem. Soc. Trans. **46**, 467 (2018).

[10] J.R. Reimers, Z.L. Cai, R. Kobayashi, M. Rätsep, A. Freiberg, and E. Krausz, Sci. Rep. **3**, 1 (2013).

[11] Y. Song, A. Schubert, E. Maret, R.K. Burdick, B.D. Dunietz, E. Geva, and J.P. Ogilvie, Chem. Sci. **10**, 2143 (2019).

[12] J.R. Reimers, M. Biczysko, D. Bruce, D.F. Coker, T.J. Frankcombe, H. Hashimoto, J. Hauer, R. Jankowiak, T. Kramer, J. Linnanto, F. Mamedov, F. Müh, M. Rätsep, T. Renger, S. Styring, J. Wan, Z. Wang, Z.Y. Wang-Otomo, Y.X. Weng, C. Yang, J.P. Zhang, A. Freiberg, and E. Krausz, Biochim. Biophys. Acta - Bioenerg. **1857**, 1627 (2016).

[13] C.C. Gradinaru, I.H.M. Van Stokkum, A.A. Pascal, R. Van Grondelle, and H. Van Amerongen, J. Phys. Chem. B **104**, 9330 (2000).

[14] H.A. Frank, A. Cua, V. Chynwat, A. Young, D. Gosztola, and M.R. Wasielewski, Photosynth. Res. **41**, 389 (1994).

[15] A. V. Ruban, R. Berera, C. Ilioaia, I.H.M. van Stokkum, J.T.M. Kennis, A.A. Pascal, H. van Amerongen, B. Robert, P. Horton, and R. van Grondelle, Nature **450**, 575 (2007).

[16] T.K. Ahn, T.J. Avenson, M. Ballottari, Y.C. Cheng, K.K. Niyogi, R. Bassi, and G.R. Fleming, Science **320**, 794 (2008).

[17] M. Son, A. Pinnola, R. Bassi, and G.S. Schlau-Cohen, Chem **5**, 575 (2019).

[18] H. Staleva, J. Komenda, M.K. Shukla, V. Šlouf, R. Kanâ, T. Polívka, and R. Sobotka, Nat. Chem. Biol. **11**, 287 (2015).

[19] P. Skotnicová, H. Staleva-Musto, V. Kuznetsova, D. Bína, M.M. Konert, S. Lu, T. Polívka, and R. Sobotka, Nat. Commun. **12**, 1 (2021).

[20] H. van A. and and R. van Grondelle, J. Phys. Chem. B **105**, 604 (2000).

[21] S. Bode, C.C. Quentmeier, P.-N. Liao, N. Hafi, T. Barros, L. Wilk, F. Bittner, and P.J. Walla, Proc. Natl. Acad. Sci. **106**, 12311 (2009).

[22] C.-P. Holleboom and P.J. Walla, Photosynth. Res. **119**, 215 (2013).

[23] Y. Miloslavina, A. Wehner, P.H. Lambrev, E. Wientjes, M. Reus, G. Garab, R. Croce, and A.R. Holzwarth, FEBS Lett. **582**, 3625 (2008).

[24] M.G. Müller, P. Lambrev, M. Reus, E. Wientjes, R. Croce, and A.R. Holzwarth, ChemPhysChem **11**, 1289 (2010).

[25] M. Wahadoszamen, R. Berera, A.M. Ara, E. Romero, and R. van Grondelle, Phys. Chem. Chem. Phys. **14**, 759 (2011).

[26] J. Kromdijk, K. Głowacka, L. Leonelli, S.T. Gabilly, M. Iwai, K.K. Niyogi, and S.P. Long, Science **354**, 857 (2016).

[27] K. Głowacka, J. Kromdijk, K. Kucera, J. Xie, A.P. Cavanagh, L. Leonelli, A.D.B. Leakey, D.R. Ort, K.K. Niyogi, and S.P. Long, Nat. Commun. **9**, 1 (2018).

[28] B. Demmig-Adams, G. Garab, W.W. Adams III, and Govindjee, *Non-Photochemical Quenching and Energy Dissipation in Plants, Algae and Cyanobacteria*, 1st ed. (Springer, 2014).

[29] I. Moya, M. Silvestri, O. Vallon, A. Gianfelice Cinque, and Roberto Bassi, Biochemistry **40**, 12552 (2001).

[30] G. De La Cruz Valbuena, F.V.A. Camargo, R. Borrego-Varillas, F. Perozeni, C. D'Andrea, M. Ballottari, and G. Cerullo, J. Phys. Chem. Lett. **10**, 2500 (2019).

[31] M. Ballottari, M.J.P. Alcocer, C. D'Andrea, D. Viola, T.K. Ahn, A. Petrozza, D. Polli, G.R. Fleming, G. Cerullo, and R. Bassi, Proc. Natl. Acad. Sci. U. S. A. **111**, E2431 (2014).

[32] R. Berera, R. van Grondelle, and J.T.M. Kennis, Photosynth. Res. **101**, 105 (2009).

[33] V. Mascoli, N. Liguori, P. Xu, L.M. Roy, I.H.M. van Stokkum, and R. Croce, Chem **5**, 2900 (2019).

[34] P.H. Lambrev, P. Akhtar, and H.S. Tan, Biochim. Biophys. Acta - Bioenerg. **1861**, 148050 (2020).

[35] G.S. Schlau-Cohen, T.R. Calhoun, N.S. Ginsberg, E.L. Read, M. Ballottari, R. Bassi, R. Van Grondelle, and G.R. Fleming, J. Phys. Chem. B **113**, 15352 (2009).

[36] M. Maiuri, J. Réhault, A.M. Carey, K. Hacking, M. Garavelli, L. Lüer, D. Polli, R.J. Cogdell,

and G. Cerullo, J. Chem. Phys. **142**, 212433 (2015).

[37] S. Park, C.J. Steen, D. Lyska, A.L. Fischer, B. Endelman, M. Iwai, K.K. Niyogi, and G.R. Fleming, Proc. Natl. Acad. Sci. U. S. A. **116**, 3385 (2019).

[38] M. Son, A. Pinnola, S.C. Gordon, R. Bassi, and G.S. Schlau-Cohen, Nat. Commun. **11**, 1 (2020).

[39] M. Son, R. Moya, A. Pinnola, R. Bassi, and G.S. Schlau-Cohen, J. Am. Chem. Soc. **143**, 17577 (2021).

[40] P. Arnoux, T. Morosinotto, G. Saga, R. Bassi, and D. Pignol, Plant Cell **21**, 2036 (2009).

[41] M. Fan, M. Li, Z. Liu, P. Cao, X. Pan, H. Zhang, X. Zhao, J. Zhang, and W. Chang, Nat. Struct. Mol. Biol. 2015 229 **22**, 729 (2015).

[42] Z. Guardini, M. Bressan, R. Caferri, R. Bassi, and L. Dall'Osto, Nat. Plants **6**, 303 (2020).

[43] B. Demmig-Adams, Biochim. Biophys. Acta - Bioenerg. **1020**, 1 (1990).

[44] H.Y. Yamamoto, T.O.M. Nakayama, and C.O. Chichester, Arch. Biochem. Biophys. **97**, 168 (1962).

[45] A.J. Young and H.A. Frank, J. Photochem. Photobiol. B Biol. **36**, 3 (1996).

[46] C. D'Andrea, D. Pezzoli, C. Malloggi, A. Candeo, G. Capelli, A. Bassi, A. Volonterio, P. Taroni, and G. Candiani, Photochem. Photobiol. Sci. **13**, 1680 (2014).

[47] F.V.A. Camargo, F. Perozeni, G. de la C. Valbuena, L. Zuliani, S. Sardar, G. Cerullo, C. D'Andrea, and M. Ballottari, J. Phys. Chem. Lett. **12**, 6895 (2021).

[48] E. Elias, N. Liguori, Y. Saga, J. Schäfers, and R. Croce, Biomacromolecules **22**, 3313 (2021).

[49] J.J. Snellenburg, S. Laptenok, R. Seger, K.M. Mullen, and I.H.M. van Stokkum, J. Stat. Softw. **49**, 1 (2012).

[50] T. Polívka and V. Sundström, Chem. Rev. **104**, 2021 (2004).

[51] X. Su, J. Ma, X. Wei, P. Cao, D. Zhu, W. Chang, Z. Liu, X. Zhang, and M. Li, Science **357**, 815 (2017).

[52] F. Passarini, E. Wientjes, H. van Amerongen, and R. Croce, Biochim. Biophys. Acta - Bioenerg. **1797**, 501 (2010).

[53] B. van Oort, L.M. Roy, P. Xu, Y. Lu, D. Karcher, R. Bock, and R. Croce, J. Phys. Chem. Lett. **9**, 346 (2018).

[54] T. Polívka and H.A. Frank, Acc. Chem. Res. **43**, 1125 (2010).

[55] M. Mozzo, L. Dall'Osto, R. Hienerwadel, R. Bassi, and R. Croce, J. Biol. Chem. **283**, 6184 (2008).

[56] L. Cupellini, S. Jurinovich, I.G. Prandi, S. Caprasecca, and B. Mennucci, Phys. Chem. Chem. Phys. **18**, 11288 (2016).

[57] S. Park, A.L. Fischer, C.J. Steen, M. Iwai, J.M. Morris, P.J. Walla, K.K. Niyogi, and G.R. Fleming, J. Am. Chem. Soc. **140**, 11965 (2018).

[58] C.C. Gradinaru, A.A. Pascal, F. van Mourik, B. Robert, P. Horton, A. Rienk van Grondelle, and H. van Amerongen, Biochemistry **37**, 1143 (1998).

[59] J.M. Salverda, M. Vengris, B.P. Krueger, G.D. Scholes, A.R. Czarnoleski, V. Novoderezhkin, H. van Amerongen, and R. van Grondelle, Biophys. J. **84**, 450 (2003).

[60] N.S. Ginsberg, J.A. Davis, M. Ballottari, Y.-C. Cheng, R. Bassi, and G.R. Fleming, Proc. Natl. Acad. Sci. **108**, 3848 (2011).

[61] Z. Guardini, M. Bressan, R. Caferri, R. Bassi, and L. Dall'Osto, Nat. Plants **6**, 303 (2020).

[62] R. Bassi, R. Croce, D. Cugini, and D. Sandonà, Proc. Natl. Acad. Sci. **96**, 10056 (1999).

[63] D. Gosztola, H. Yamada, and M.R. Wasielewski, J. Am. Chem. Soc. **117**, 2041 (1995).

[64] J.L. Herek, M. Wendling, Z. He, T. Polívka, G. Garcia-Asua, R.J. Cogdell, C.N. Hunter, R. Van Grondelle, V. Sundström, and T. Pullerits, J. Phys. Chem. B **108**, 10398 (2004).

[65] H. Cong, D.M. Niedzwiedzki, George N. Gibson, and H.A. Frank, J. Phys. Chem. B **112**, 3558 (2008).

[66] D. Niedzwiedzki, J.F. Koscielecki, H. Cong, J.O. Sullivan, G.N. Gibson, R.R. Birge, and Harry

A. Frank, J. Phys. Chem. B **111**, 5984 (2007).

[67] D.S. Larsen, E. Papagiannakis, I.H.M. Van Stokkum, M. Vengris, J.T.M. Kennis, and R. Van Grondelle, Chem. Phys. Lett. **381**, 733 (2003).

[68] D.M. Niedzwiedzki, J.O. Sullivan, T. Polívka, A. Robert, R. Birge, and A.F. Harry, J. Phys. Chem. B **110**, 22872 (2006).

[69] E. Papagiannakis, J.T.M. Kennis, I.H.M. van Stokkum, R.J. Cogdell, and R. van Grondelle, Proc. Natl. Acad. Sci. **99**, 6017 (2002).

[70] E. Papagiannakis, S.K. Das, A. Gall, I.H.M. van Stokkum, B. Robert, R. van Grondelle, Harry A. Frank, and J.T.M. Kennis, J. Phys. Chem. B **107**, 5642 (2003).

[71] F. Saccon, M. Durchan, D. Bína, C.D.P. Duffy, A. V. Ruban, and T. Polívka, IScience **23**, 101430 (2020).

[72] N. Liguori, P. Xu, I.H.M. Van Stokkum, B. Van Oort, Y. Lu, D. Karcher, R. Bock, and R. Croce, Nat. Commun. **8**, 1 (2017).

[73] P.O. Andersson and T. Gillbro, J. Chem. Phys. **103**, 2509 (1998).

[74] C.C. Gradinaru, J.T.M. Kennis, E. Papagiannakis, I.H.M. Van Stokkum, R.J. Cogdell, G.R. Fleming, R.A. Niederman, and R. Van Grondelle, Proc. Natl. Acad. Sci. U. S. A. **98**, 2364 (2001).

[75] V. Balevičius, T. Wei, D. Di Tommaso, D. Abramavicius, J. Hauer, T. Polívka, and C.D.P. Duffy, Chem. Sci. **10**, 4792 (2019).

[76] R. Bassi and L. Dall'Osto, Annu. Rev. Plant Biol. **72**, 47 (2021).

[77] L. Dall'Osto, S. Caffarri, and R. Bassi, Plant Cell **17**, 1217 (2005).